VII International Conference on Computational Methods in Marine Engineering

MARINE 2017

Nantes, France
May 15 – 17, 2017

A publication of:

International Center for Numerical Methods in Engineering (CIMNE)
Barcelona, Spain

Printed by: Artes Gráficas Torres S.L., Huelva 9, 08940 Cornellà de Llobregat, Spain

ISBN: 978-84-946909-8-3

VII International Conference on Computational Methods in Marine Engineering
MARINE 2017
M. Visonneau, P. Queutey and D. Le Touzé (Eds)

THE DVH MODEL: SIMULATING 2D VISCOUS FLOWS AROUND FIVE DIFFERENT BODIES AT RE=10,000

Emanuele ROSSI*, Andrea COLAGROSSI†, David LE TOUZÉ*

* École Centrale Nantes, LHEEAresearch department (ECN/CNRS), Nantes, France

† CNR - INSEAN, Via di Vallerano, Rome, Italy

Key words: Viscous flow around blunt bodies, wing profile in stall condition, Particle Vortex Method, Diffused Vortex Hydrodynamic, vortical wakes.

Abstract. The Diffused Vortex Hydrodynamic (DVH) is a meshless 2D Lagrangian incompressible Particle Vortex Method. In this study the DVH will be applied to simulate viscous flows around five different bodies at Re=10,000. In order to show how the DVH method works, simulations about five different geometries will be discussed: (i) a cylinder with circular section, (ii) a cylinder with squared section, (iii) a narrow elliptical profile, (iv) a thick elliptical profile and (v) a NACA0010 profile. All the five considered geometries develop a complex vortical wake and, moreover, the last three profiles, having a 30 degrees angle of attack, give rise to flow separation on the suction side.

1 Introduction

The study describes an improved meshless 2D Lagrangian incompressible Particle Vortex Method called Diffused Vortex Hydrodynamic (DVH). Deeply described and validated ([1, 2, 3, 4]), the method will be briefly presented in the following section.

The DVH method brings the following advantages:

(I) the continuity equation is automatically satisfied;

(II) the pressure field is no longer a direct unknown of the problem, thanks to the vorticity formulation of the Navier-Stokes equation;

(III) the vorticity formulation allows to discretize only the rotational region of the flow (self-adaptivity);

(IV) high accuracy on the velocity field evaluation (obtained through a spatial integration);

(V) boundary conditions at infinity are automatically satisfied;

(VI) the Lagrangian nature of the method, compared to mesh-based approaches, reduces the numerical dissipation due to NavierStokes equations non-linear term.

However, the Lagrangian nature of this method needs the introduction of redistribution techniques to preserve accuracy (see *e.g.* [5]).

The DVH method is coupled with a low CPU costs packing algorithm [6] which generate a "Regular Point Distribution" (RPD) close to a solid surface. DVH is a body-fitted method and thanks to the RDPs the velocity boundary condition are enforced exactly on the body surface, therefore .

This model is particularly suited to get a correct description of the vortical fluid motion around a body of complex geometry.

To show the DVH method ability in solving complex flows, five different body geometries at Re=10,000 will be discussed.

2 The DVH method.

The DVH is governed by the Navier-Stokes equation written in vorticity formalism:

$$\frac{D}{Dt}\omega = \nu\Delta\omega \qquad \forall \mathbf{r} \in \Omega, \tag{1}$$

where D/Dt is the time material derivative, ω is the vorticity, ν is the kinematic viscosity and Ω is the domain of the 2D viscous incompressible flow.

In order to solve eq. 1 at each time step the operator splitting scheme [7, 8] will be used. To obtain the numerical solution is necessary to solve an inviscid advective step governed by the Euler equation:

$$\frac{D}{Dt}\omega(\mathbf{r}, t) = 0 \tag{2}$$

together with a purely diffusive step governed by the heat equation:

$$\frac{\partial}{\partial t}\omega(\mathbf{r}, t) = \nu\Delta\omega(\mathbf{r}, t). \tag{3}$$

The presence of a body within the flow field requires to add a specific process, between the advective and the diffusive steps, generating vorticity on the body contour in order to enforce the no slip boundary condition.

The vorticity field is discretised as a sum of N vortices, each of them represented by a positive smooth approximation of the Dirac δ distribution, δ_ϵ, and a circulation Γ_i:

$$\omega(\mathbf{r}, t) = \sum_{i=1}^{N} \Gamma_i(t)\delta_\epsilon(\mathbf{r} - \mathbf{r}_i). \tag{4}$$

Before starting the simulation the Packing algorithm described in [6] is used to generate a set of points regularly distributed (RPD) around the solid body. This procedure allows to arrange points around complex contours, while preserving the volume around each point.

During the advective step the velocity field is decomposed as follows:

$$\mathbf{u} = \mathbf{u}_\infty + \mathbf{u}_\omega + \mathbf{u}' \tag{5}$$

where $\mathbf{u}_\infty$ is the free stream velocity, $\mathbf{u}_\omega$ is the velocity induced by the vortex particles, while $\mathbf{u}'$ is the contribution due to the presence of the body within the flow. The velocity $\mathbf{u}_\omega$ can be evaluated using the Biot-Savart law, written as:

$$\mathbf{u}_\omega(\mathbf{r}, t) = \sum_{i=1}^{N} \Gamma_i(t) \mathbf{K}_\epsilon(\mathbf{r}, \mathbf{r}_i) \tag{6}$$

where $\mathbf{K}_\epsilon$ is the mollified Biot-Savart kernel.

To evaluate the term $\mathbf{u}'$ the body is discretised using a set of sources and point vortices. From $\mathbf{u}'$ it is also possible to generate a new set of vortices on the body surface, enforcing the no-slip boundary condition exactly on its contour.

A Fast Multiple Method (FMM) is used to speed up the evaluation of the velocity $\mathbf{u}$.

The vortices are displaced using a fourth order Runge-Kutta algorithm.

The diffusive step is performed following the deterministic algorithm described in [9]: each vortex particle gives a vorticity contribution on the RPDs by a superposition of elementary solutions of the heat equation (see [1, 3]). The set of points created during the diffusion process become the new set of vortex particles overwriting the previous one. The use of RPDs during diffusion impedes the excessive clustering or rarefaction of the vortex particles and avoids the use of remeshing procedures.

In order to solve the diffusion near a smooth solid boundary, an homogeneous Neumann condition for the vorticity field, together with a flat plate approximation of the solid contour, will be used. This approximation is no longer valid if the body has geometrical singularities. In this case is necessary to introduce a suitable visibility mask as explained in [3].

Another characteristic of the DVH method is the multi-resolution approach. That implies using several overlapping RPDs, which spatial resolution decreases as the distance from the body increase (see [2]).

3 Flow around a circular cylinder at Re=10,000.

In the present section the DVH simulation of the flow past a circular cylinder at Re=10,000 will be discussed. The considered cylinder has a diameter equal to c and the Reynold number is defined as $\mathrm{Re} = Uc/\nu$, where U is the free stream velocity.

As discussed in [10], in a two dimensional framework the flow for a cylinder at Re=10,000 remain at a lower sub-critical regime: the shear layers start to fluctuate and only few eddies are formed downstream. As visible in the left plot of figure 1, the first seconds of the simulation are characterized by the formation of two vortical structures in the recirculation areas behind the cylinder. It is also possible to notice the formation of small eddies in the near wake due to the shear layer dynamic. The two recirculation bubbles remain stable until $tU/c = 10$. After this time the wake becomes unstable and the shedding mechanism begins, in which shed eddies form dipole structures downstream in the wake. Moreover, center and right plots of Figure 1 depict the vorticity field in the near wake region at the minimum and maximum of the lift.

The shedding mechanism induces oscillations on the forces, more visible on the lift than on the drag. The time evolution of lift and drag coefficients are reported in figure 2. The latter are defined as:

$$C_d = F_x/(1/2 \rho U^2 c) \qquad C_l = F_y/(1/2 \rho U^2 c) \tag{7}$$

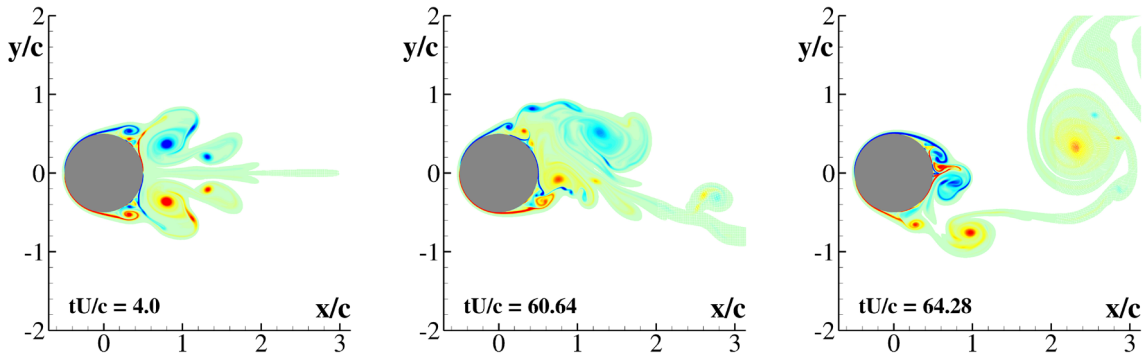

Figure 1: Flow past a cylinder at Re=10,000. Left: recirculation of the shear layer at the beginning of the simulation. Center: vorticity field near the body at minimum lift. Right: vorticity field near the body at maximum lift. The dimensionless vorticity $\omega c/U$ scales from -40 to 40.

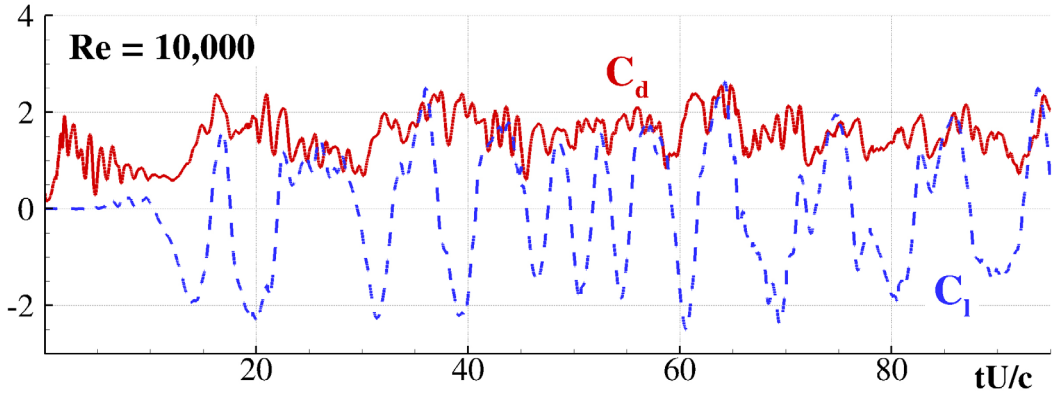

Figure 2: Flow past a cylinder at Re=10,000: lift and drag coefficients time histories.

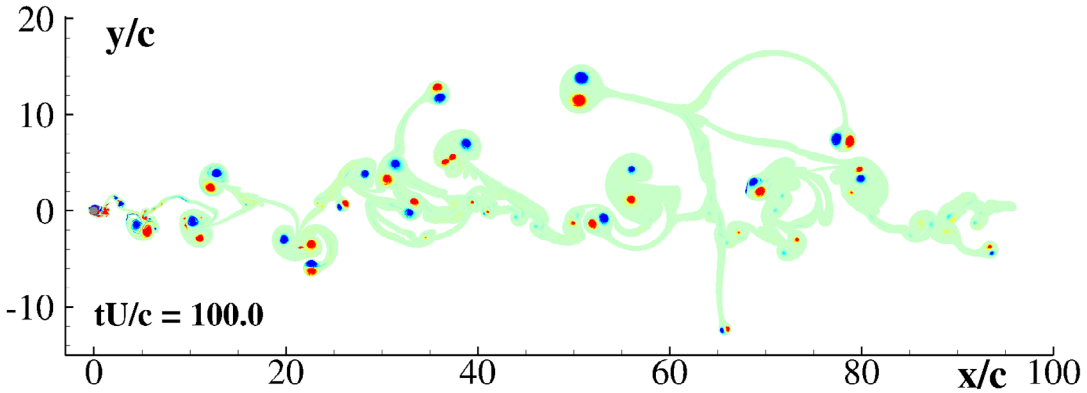

Figure 3: Wake at the end of the simulation for the cylinder at Re=10,000. The dimensionless vorticity $\omega c/U$ scales from -40 to 40

where ρ is the fluid density.

At this Reynolds number the forces time behaviour is aperiodic. Because of the aperiodic behaviour of the shedding mechanism each eddies shed have a different intensity and the wake is irregular as shown in Figure 3.

4 Flow around a square cylinder at Re=10,000.

This section study the flow past a square cylinder at Re=10,000. The length of the side is indicated with c. The DVH method can solve highly complicated flows, as visible from the beginning of the simulation.

Starting the simulation, the flow separates at each of the four vertices, and that generates four thin shear layers, as shown in left plot of Figure 4.

The shear layers detaching from the front part of the body directly induce a backward flow on the two side of the square cylinder parallel to the free stream direction, causing a local change of sign in the vorticity field. As a consequence of the interaction of positive and negative vorticity on the horizontal faces of the cylinder, small eddies are generated and convected downstream. Moreover, the detached shear layers roll up at the back of the square, forming two recirculation bubbles. Once the front detached eddies cover the whole length of the square cylinder, no more shear layer will be detached from the back of the body, interrupting the growth of the recirculation bubbles, as in the center plot of Figure 4. Continuing the simulation, just small eddies are detached from the body, not only from the horizontal faces but also from the back one, as visible in right plot of Figure 4.

Because of the detaching of small eddies, no principal shedding mechanism can be observed as well as in the lift and drag coefficients time histories (Figure 5).

The absence of regular shedding of large eddies is visible also on the wake (Figure 6). The wake is mainly formed by small eddies, and, however, while these eddies move inside the wake they interact with each other merging and forming dipole structures. For this geometry the wake appears more compact in space than the wake shed of the circular cylinder (see Figure 3).

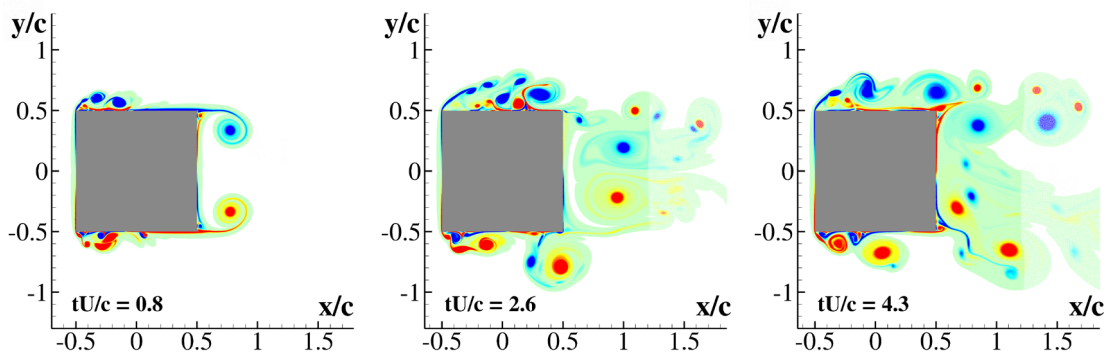

Figure 4: Simulation initial stages of the flow past a square cylinder at Re=10,000. The dimensionless vorticity $\omega c/U$ scales from -40 to 40.

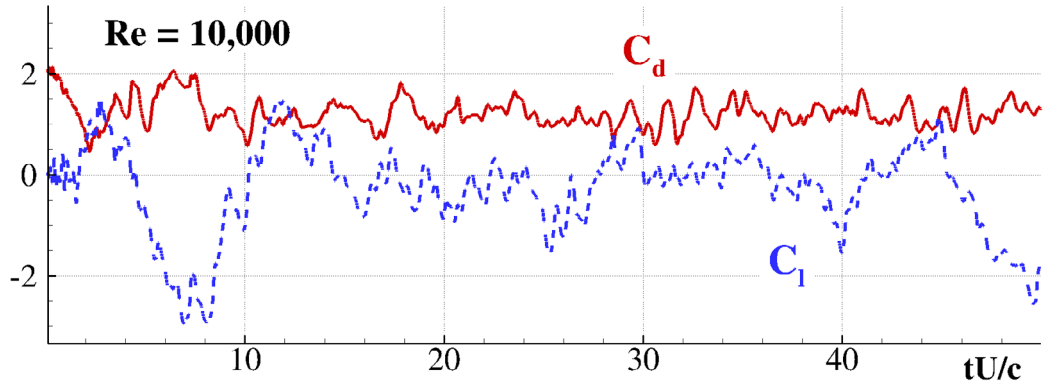

Figure 5: Flow past a square cylinder at Re=10,000. Lift and drag coefficients time histories.

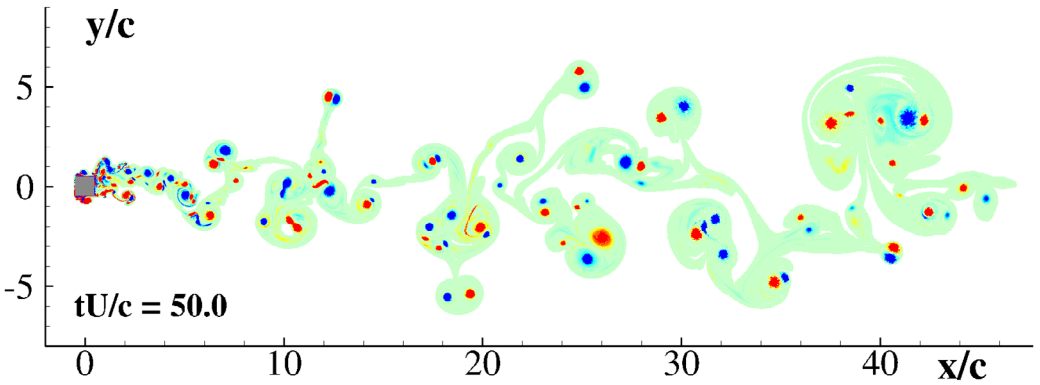

Figure 6: Wake at the end of the simulation for the square cylinder at Re=10,000. The dimensionless vorticity $\omega c/U$ scales from -40 to 40.

5 Flow around three different airfoils at Re=10,000 in stall condition.

In this section three different airfoils at Re=10,000 and angle of attack $\alpha = 30°$ are considered:

(i) a thick elliptical profile with aspect ratio between minor axis, b, and the major axis, c, equal to $b/c = 0.25$;

(ii) a narrow elliptical profile with aspect ratio $b/c = 0.1$;

(iii) a NACA0010 profile with chord c.

The viscous flows around these three geometries at Re=10,000 are characterized by the formation of shear layers detaching from the leading and the trailing edge. At the considered viscosity level, the shear layers roll up mechanism takes place.

The shear layer detaching from the trailing edge could also become unstable during the roll-up, generating a series of small eddies, usually called secondary vortices, as shown in left plot of Figure 7.

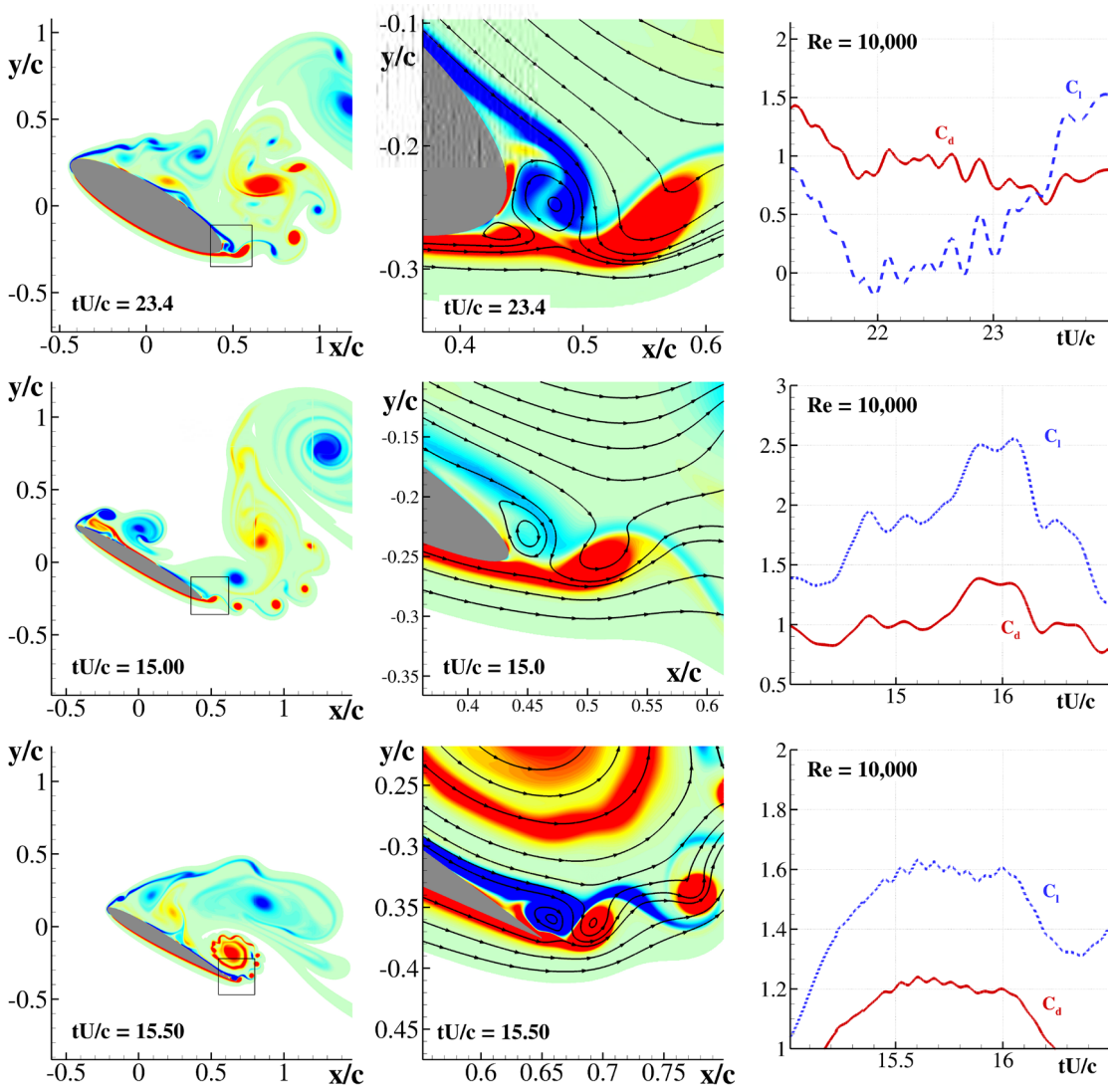

Figure 7: From top to bottom: detail of the vorticity field near the airfoils and of the loads. Left: vorticity field near the airfoil with the formation of secondary vortices. Center: detail of the vorticity field with the vorticity structure responsible for the shedding of the secondary vortices. Right: detail of the loads during the shedding of the secondary vortices. The dimensionless vorticity $\omega c/U$ in the vorticity fields plots scales from -40 to 40.

The mechanism of formation of these secondary vortices at Re=10,000 has been described in [11], [12] and [13]. The trailing edge anti-clockwise vortex, in some cases, could interact with the boundary layer on the suction side of the body. If this happened, a local acceleration of the flow, generating a small clockwise vorticity structure on the trailing edge, can be observed. The clockwise vorticity structure is unstable and with a periodical oscillation, leading to the fragmentation of the counter-clockwise shear layer.

The above mentioned mechanism is shown in Figure 7: in the left plots the fragmentation of the counter-clockwise shear layer is visible in all the considered geometries; in the central plots the specific behaviour on the trailing edge is highlighted.

Secondary vortices mechanism influences also lift and drag forces, introducing components with high frequency and low intensity, as reported in the right plots of Figure 7.

Moreover, time histories of the drag and lift coefficients are presented in left plots of Figure 8. The force time signals have a complex evolution with different frequency components and absence of periodicity.

As a results of the above mechanism the wake are more complex, that means that during the wake evolution dipole structures, generated by the leading and trailing edge shear layers, interact with secondary vortices.

The ability of the DVH to simulate long wakes with complicated vorticity field is well represented in right plot of Figure 9.

The wake is formed by a series of dipole structures travelling upwards together with secondary structures travelling in the free stream direction.

As reported in Figure 9, the thikness of the considered bodies can influence the vorticity field, for example, the thick ellipse wake is characterized by larger wave numbers (i.e. larger vortex scales), compared to the other two profiles.

6 Conclusions

The DVH method, as in [1, 2, 3, 10] as well as in this article,is particularly suited in dealing with complex and/or narrow body geometries with vertices, especially because of its ability to solve and get a correct description of the 2D vortical fluid motion around body of complex geometry.

The study focused on DVH simulations at Re=10,000. At this viscosity level the vortex dynamic in the wake region has a complex nature while on the other hand the Reynolds number is too low to allow the transition to turbulence regimes. In such conditions numerical simulations can be quite challenging because boundary layers as well as near wake regions need to be properly resolved. Thanks to its characteristics, the DVH can be applied to solve these kind of challenging Reynolds numbers flows.

Moreover, DVH can be a useful tool in analysing viscous regime, as previously discussed, and be of interest in the context of maritime engineering when considering, for example, control surfaces of unmanned underwater vehicles (UUV) (see *e.g.* [14, 15, 16]) or problem related to Vortex Induced Vibrations of Marine Risers (see *e.g.* [17, 18]).

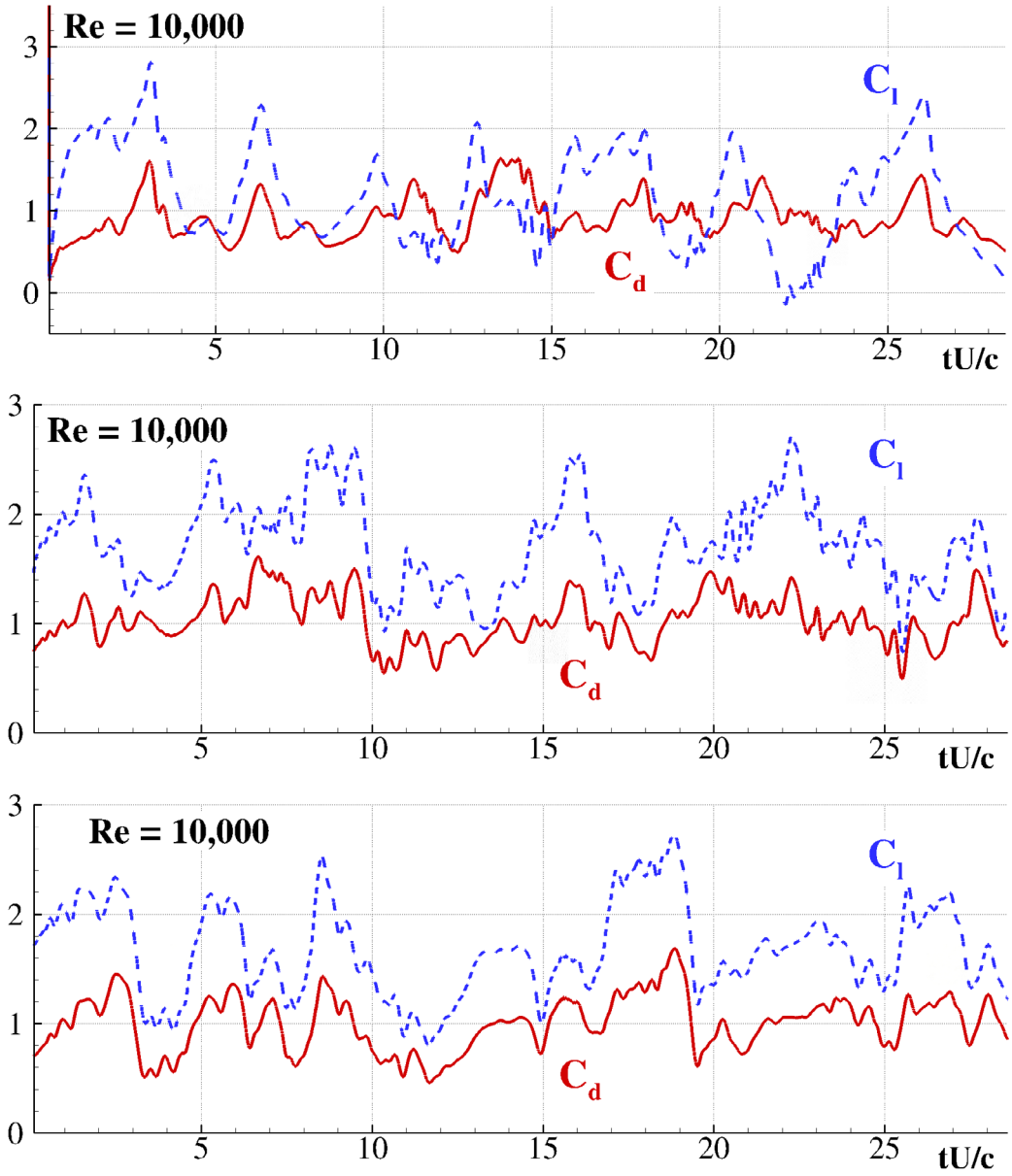

Figure 8: From top to bottom: Lift and Drag coefficient time histories for the ellipse with aspect ratio 0.25, the ellipse with aspect ratio 0.1 and the NACA0010 respectively.

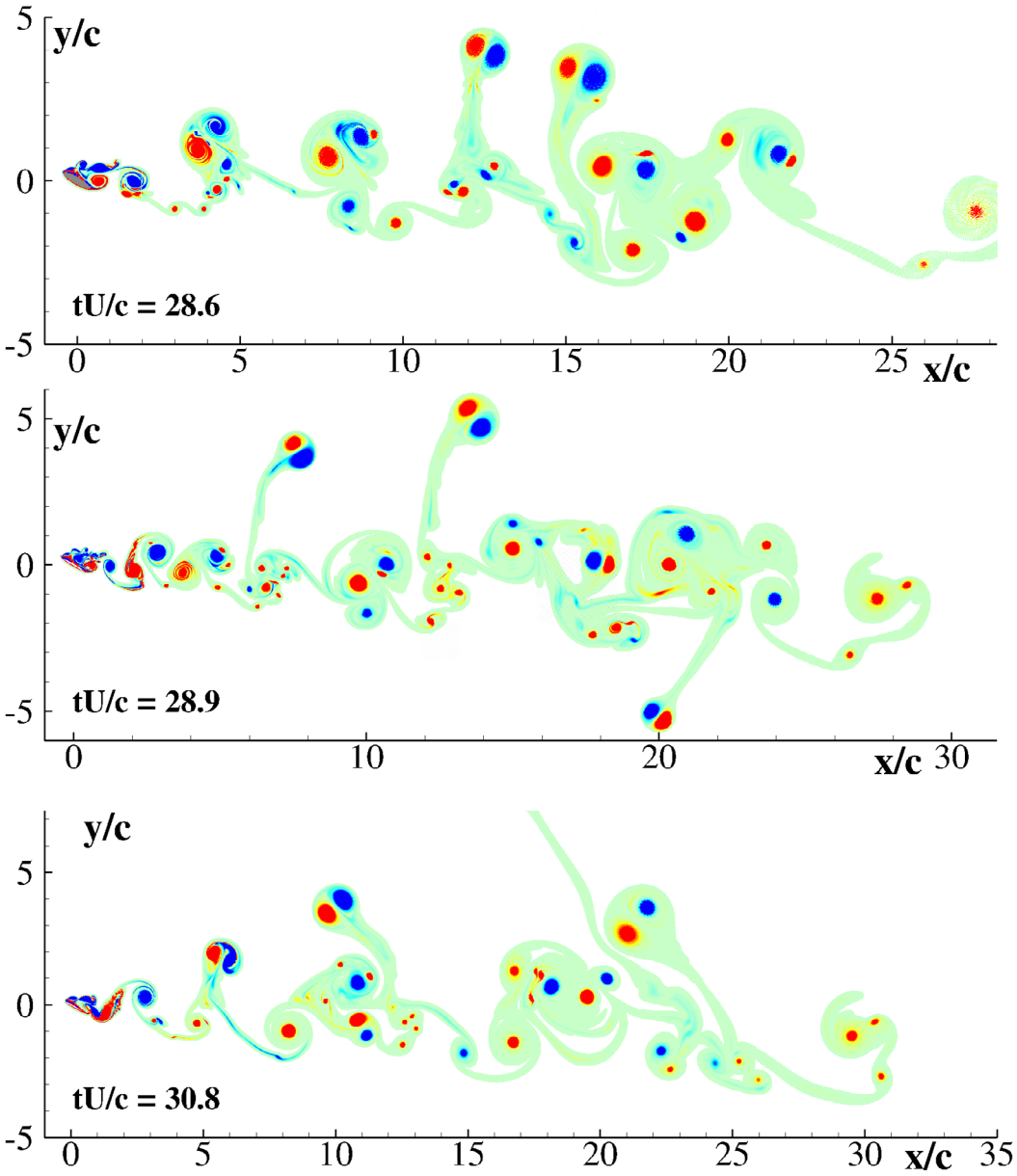

Figure 9: From top to bottom: vorticity field at the end of the simulation for the ellipse with aspect ratio 0.25, the ellipse with aspect ratio 0.1 and the NACA0010 respectively. The dimensionless vorticity $\omega c/U$ scales from -2 to 2.

Acknowledgements

This work has been partially supported by the Flagship Project RITMARE - Italian Research for the Sea - coordinated by Italian National Research Council and funded by Italian Ministry of Education, University and Research within Nat. Res. Program 2015-2016, and has received a post-doctoral grant from Ecole Central Nantes.

REFERENCES

[1] Rossi, E., Colagrossi, A. and Graziani, G. *Numerical simulation of 2D-vorticity dynamics using particle methods*. Computers & Mathematics with Applications, 69(12): 1484-1503, 2015.

[2] Rossi, E., Colagrossi, A., Bouscasse, B. and Graziani, G. *The Diffused Vortex Hydrodynamics method*. Communications in Computational Physics, 18(2): 351-379, 2015.

[3] Rossi, E., Colagrossi, A., Durante, D. and G. Graziani, *Simulating 2D viscous flow around geometries with vertices through the Diffused Vortex Hydrodynamics method*. Computer Methods in Applied Mechanics and Engineering, 302: 147-169, 2016.

[4] Colagrossi, A., Rossi, E., Marrone, S. and Le Touzé,D. *Particle Methods for Viscous Flows: Analogies and Differences Between the SPH and DVH Methods*. Communications in Computational Physics, 20(3) pp. 660-688, 2016.

[5] Barba, L.A., Leonard, A. and Allen, C.B. *Numerical investigations on the accuracy of the vortex method with and without remeshing*. AIAA paper 3426, 2003.

[6] Colagrossi, A., Bouscasse, B., Antuono, M. and Marrone, S. *Particle packing algorithm for SPH schemes*. Computer Physics Communications 183(2), pp. 1641-1683, 2012.

[7] Chorin, A. *Numerical study of slightly viscous flow*. Journal of Fluid Mechanics, 57(04): 785796, 1973.

[8] Chorin, A. *Vortex sheet approximation of boundary layers*. Journal of Computational Physics, 27(3): 428442, 1978.

[9] Benson, M.G., Bellamy-Knights, P.G., Gerrard, J.H. and Gladwell, I. *A viscous splitting algorithm applied to low Reynolds number flows round a circular cylinder*. Journal of Fluids and Structures, 3(5): 439479, 1989.

[10] Durante, D., Rossi, E., Colagrossi, A. and Graziani, G. *Numerical simulations of the transition from laminar to chaotic behaviour of the planar vortex flow past a circular cylinder*. Communications in Nonlinear Science and Numerical Simulation, 2016.

[11] Wang, Z. J., Liu, J. G., and Childress, S. *Connection between corner vortices and shear layer instability in flow past an ellipse*. Physics of Fluids, 11(9):2446-2448, 1999.

[12] Kudela, H., and Kozłowski, T. *Vortex in cell method for exterior problems*. Journal of Theoretical and Applied Mechanics, 47(4):779-796, 2009.

[13] Luchini, P., and Tognaccini, R. *Viscous and inviscid simulations of the start-up vortex.* Journal of Fluid Mechanics, 813:53-69, 2017.

[14] Suzuki, H., Kato, N., Katayama, T., and Fukui, Y., *Motion Simulation of an Underwater Vehicle with Mechanical Pectoral Fins Using a CFD-based Motion Simulator*, Proc. of Symposium on Underwater Technology and Workshop on Scientific Use of Submarine Cables and Related Technologies, Tokyo, pp. 384-390, 2007.

[15] Palmisano, J., Geder, J., Ramamurti, R., Liu, K.J., Cohen, J.J., Mengesha, T., Naciri, J., Sandberg, W., and Ratna, B., *Design, Development, and Testing of Flapping Fins with Actively Controlled Curvature for an Unmanned Underwater Vehicle*, in "Bio-mechanisms of Swimming and Flying: Fluid Dynamics, Biomimetic Robots, and Sports Science", Ed. Kato, Naomi and Kamimura, Shinji, pp 283–294, Springer Japan, 2008.

[16] Hwang, Y.L. *Hydrodynamic modeling of LMRS unmanned underwater vehicle and tow tank test validation*, Oceans 2003. Celebrating the Past ... Teaming Toward the Future, San Diego, CA, USA, pp. 1425-1430, Vol.3., 2003

[17] Swithenbank, S.B.,Vandiver, J.K., Larsen, C.M. and Lie, H., *Reynolds number dependence of flexible cylinder VIV response data*, Proc. of the ASME 27th International Conference on Offshore Mechanics and Arctic Engineering (OMAE) June 15-20, Estoril, Portugal, 2008.

[18] Resvanis, T.L., Jhingran, V., Vandiver, J.K., and Liapis, S., *Reynolds number effects on the vortex-induced vibration of flexible marine risers*, Proc. of the ASME 31st International Conference on Ocean, Offshore and Arctic Engineering (OMAE) July 1-6, Rio de Janeiro, Brazil, 2012.